

UNPAIRED MRI SUPER RESOLUTION WITH SELF-SUPERVISED CONTRASTIVE LEARNING

Hao Li^{1,†}, Quanwei Liu^{2,5,†}, Jianan Liu^{3,*}, Xiling Liu⁴, Yanni Dong^{2,*}, Tao Huang⁵, and Zhihan Lv⁶

¹ The Department of Neuroradiology, University Hospital Heidelberg, Heidelberg, Germany;

² Institute of Geophysics and Geomatics, China University of Geosciences, Wuhan, China;

³ Vitalent Consulting, Gothenburg, Sweden;

⁴ Department of Stomatology, Shenzhen People's Hospital, Shenzhen, China;

⁵ The College of Science and Engineering, James Cook University, Cairns, Australia;

⁶ Department of Game Design, Faculty of Arts, Uppsala University, Sweden.

ABSTRACT

High-resolution (HR) magnetic resonance imaging (MRI) is crucial for enhancing diagnostic accuracy in clinical settings. Nonetheless, the inherent limitation of MRI resolution restricts its widespread applicability. Deep learning-based image super-resolution (SR) methods exhibit promise in improving MRI resolution without additional cost. However, these methods frequently require a substantial number of HR MRI images for training, which can be challenging to acquire. In this paper, we propose an unpaired MRI SR approach that employs self-supervised contrastive learning to enhance SR performance with limited training data. Our approach leverages both authentic HR images and synthetically generated SR images to construct positive and negative sample pairs, thus facilitating the learning of discriminative features. Empirical results presented in this study underscore significant enhancements in the peak signal-to-noise ratio and structural similarity index, even when a paucity of HR images is available. These findings accentuate the potential of our approach in addressing the challenge of limited training data, thereby contributing to the advancement of high-resolution MRI in clinical applications.

Index Terms— Magnetic resonance imaging, super-resolution, self-supervised, contrastive learning.

1. INTRODUCTION

Magnetic Resonance Imaging (MRI) is widely used for diagnosis and monitoring of treatment progress non-invasively [1]. However, the high cost and long scan time make it challenging to acquire high-resolution (HR) MRI images and limit the use of MRI in areas such as surgical guidance. To address this issue, single-image super-resolution

(SR) techniques have been developed using deep learning-based approaches to enhance image resolution directly from low-resolution (LR) images [2, 3, 4].

Typically, these techniques rely on convolutional neural networks (CNNs) to learn the transform from LR images to HR ones. Since super-resolution reconstruction (SRR) is a complex and challenging problem, various powerful CNN architectures have been developed to improve the effectiveness of SR [5, 6]. These supervised learning (SL) methods require a large number of paired HR and LR images. However, patient movements are always inevitable, leading to geometric distortions of soft tissues. As a result, the acquisition of aligned pairs of MRI images is extremely difficult. To solve this problem, unsupervised learning (UL) methods are adopted for MRI SRR. UL SR does not require pairs of images and achieves comparable results to supervised models in real-world image SRR [7, 8, 9, 10]. Inspired by the real-world image UL SRR methods, unsupervised MRI SR methods have been developed in response to recent advances in the field and eliminate the demand on paired training images [11, 12]. Nevertheless, they still require a significant number of HR MRI images for training, which leads to long scan times and more motion artifacts [12]. To reduce reliance on a large amount of HR MRI images, contrastive learning (CL) [13, 14] can be used to extract supervisory information from a small amount of unpaired MRI images and train the network with this self-generated supervisory information. This approach allows contrastive-based models to identify meaningful representations for unsupervised or weakly supervised MRI SR tasks.

This study presents an unpaired MRI SR framework that utilizes CL. The framework integrates InfoNCE [13] loss into an unsupervised SR architecture. Our contributions can be summarized as follows:

- We present an efficient strategy grounded in CL for unpaired MRI SRR. This strategy involves the construction of positive sample pairs between generated SR images and

[†] The first two authors contributed equally to this work.

^{*} Corresponding authors.

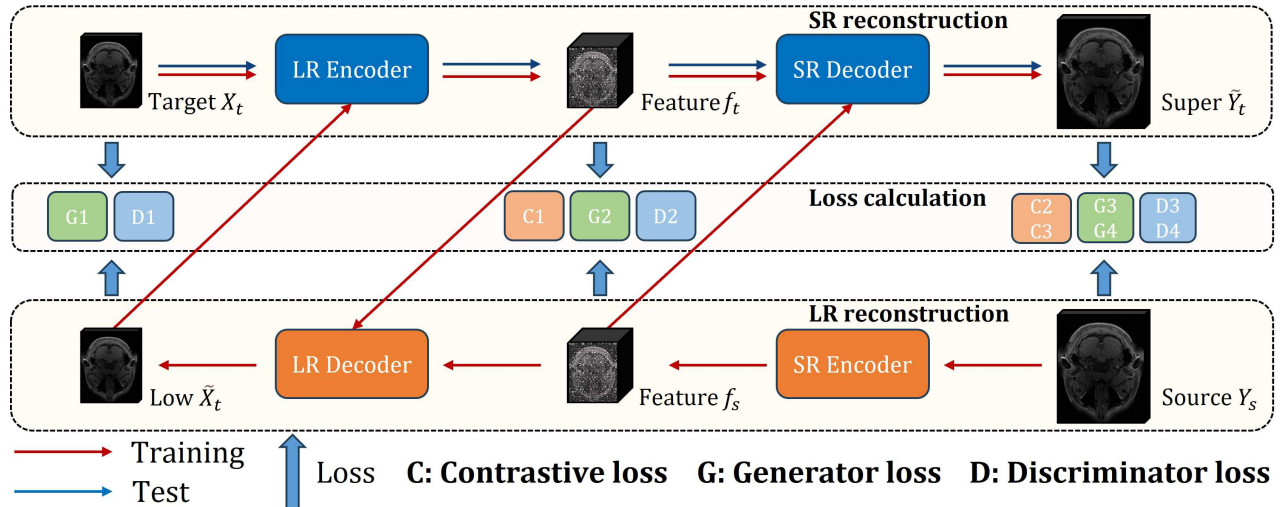


Fig. 1. The pipeline of the proposed model, where **C**, **G**, **D** are contrastive loss, generator loss, and discriminator loss. Since the above three loss functions are computed along different paths in feature space and image space respectively, we distinguish them with the corner notation. The target X_t and source Y_t are entered into the model together to train the model. The discriminator **D** is first trained according to the data flow to get the discriminative loss. Then the generator **G** and contrastive learning **C** are trained together to get the generation loss and contrastive loss. The blue arrow points to the location of the loss calculation. After training, only the LR encoder and SR decoder networks are used to infer to generate SR images.

ground truth images, while negative samples are fashioned within a batch by pairing samples with each other.

- We devise a contrastive representative learning network, which furnishes a novel and effective approach to unpaired MRI SR, even in scenarios characterized by unpaired and limited amounts of training images. In comparison to various baseline algorithms, our proposed models yield competitive outcomes.
- Experimental results manifest the enhanced stability of our model in comparison to the baseline when the number of training samples decreases. Specifically, when employing only 10% of the training dataset, our model exhibits a 0.0239 dB improvement in SSIM and a 1.1802 dB enhancement in PSNR to the baseline method.

2. PROPOSED METHOD

2.1. Contrastive Learning and Sample Generation

Self-supervised CL has become a prominent framework for acquiring invariant feature representations of data. Previous research [13, 14, 15, 16] has extensively explored image feature extraction via CL, achieving performance levels that are on par with or surpassing supervised learning in various high-level tasks like classification, semantic segmentation, and object detection. However, the conventional CL pipeline is less suitable for low-level vision tasks [17].

Traditional CL faces difficulties when dealing with low-level vision tasks like SR. The process involves creating

pairs of positive and negative samples, to reduce the distance between positive samples while increasing the separation between negative ones. However, this becomes challenging when using data augmentation to generate sequences of positive and negative sample pairs, as it can lead to issues with maintaining dense pixel correspondences. As a result, the effectiveness of the traditional CL approach is diminished. Despite this, a few studies have explored the application of CL in natural SR [18]. For instance, Wang et al. [19] used negative samples from other datasets to train their network, while CRL-SR [20] used CL to extract resolution-invariant features and recover lost or corrupted high-frequency details.

Our research introduces a simple strategy for constructing positive and negative sample pairs. As depicted in Fig. 1, we incorporate a feature contrastive loss and a reconstruction contrastive loss established between the generated feature maps (or SR images) and the extracted feature map (or ground truth).

CL is implemented using a contrastive loss, with one of the classical variants being infoNCE [13]. The work [21] modified infoNCE by introducing inter-embedding and intra-embedding terms in graph learning. For the i -th image, the loss is expressed as:

$$\mathcal{L}(u_i, v_i) = \log \frac{e^{\theta(u_i, v_i)/\tau}}{e^{\theta(u_i, v_i)/\tau} + \mathcal{L}_{te}(u_i, v_k) + \mathcal{L}_{tr}(u_i, u_k)}, \quad (1)$$

$$\mathcal{L}_{te}(u_i, v_k) = \sum_{k=1}^N \mathbb{I}_{[k \neq i]} e^{\theta(u_i, v_k)/\tau}, \quad (2)$$

$$\mathcal{L}_{tr}(u_i, u_k) = \sum_{k=1}^N \mathbb{I}_{[k \neq i]} e^{\theta(u_i, u_k)/\tau}. \quad (3)$$

Here u_i and v_i represent the nonlinear embeddings generated from training samples. $\theta(u_i, v_i)$ signifies the cosine similarity between u_i and v_i , which is equivalent to the dot product between L2-normalized u_i and v_i , e. g. $\theta(u_i, v_i) = u_i^T \cdot v_i / \|u_i^T\| \cdot \|v_i\|$. The temperature parameter τ governs the impact of penalties on hard negative samples. $\mathbb{I}_{[k \neq i]}$ acts as an indicator function. N denotes the batch size. $\mathcal{L}_{te}(u_i, v_k)$ and $\mathcal{L}_{tr}(u_i, u_k)$ pertain to inter-embedding and intra-embedding calculations, respectively. Since the two embeddings are symmetric, the final optimization goal is to minimize the average overall positive pairs:

$$\mathcal{L}_{cl} = -\frac{1}{2N} \sum_{i=1}^N [\mathcal{L}(u_i, v_i) + \mathcal{L}(v_i, u_i)]. \quad (4)$$

This formula can also be applied to CL involving images. Due to the separate calculation method, this approach is more memory-saving. Therefore, this form of contrastive loss is adopted in our study.

2.2. Unpaired MRI SR Architecture

The model comprises two main components: the representation generation module and the loss calculation module, as illustrated in Fig. 1.

The representation generation module comprises two key elements: the LR reconstruction network (depicted in orange) and the SRR network (represented in blue). The LR reconstruction network initially encodes the source domain dataset Y_s into the feature domain. Subsequently, the LR decoder network generates the LR image from the feature map f_s . In contrast, the objective of the SRR network is to extract features from the target domain dataset X_t and decode them into an SR image Y_t .

In our approach, the LR encoder consists of six identical convolution modules, each comprising a convolution layer followed by an activation layer employing the LeakyReLU function. The SR encoder shares a similar structure with the LR encoder, except for the initial convolutional layer, which employs a stride of 2 to downsample the HR MRI image to match the size of the LR feature map. We utilize a modified RCAN [22] architecture as the backbone of our SR network. This choice not only enhances computational efficiency but also ensures superior inference performance.

The loss calculation module consists of three components: the discrimination loss module (represented by **D**), the generation loss module (represented by **G**), and the contrastive loss module (represented by **C**). The discrimination loss module employs three discriminant networks, each responsible for determining the authenticity of the source domain, feature domain, and target domain. Notably, domain adaptation is integrated into this process, significantly improving

the quality of the reconstructed SR image. The generation loss module incorporates various reconstruction losses, including the L1 loss and the structural similarity (SSIM) loss, to guarantee the fidelity and perceptual quality of the generated SR images. Lastly, the contrastive loss module enhances the model’s feature extraction capability by increasing the separation between samples within the batch and reducing the distance between the generated samples and the ground truth.

For the discrimination network, we employ three VGG networks. And following the principles outlined in MoCo [13] and SimCLR [14], we encode positive and negative patches into a sequence using a six-layer convolution and a two-layer multi-layer perceptron projection head [23], which can improve the nonlinearity of the model and enhance the model performance.

3. EXPERIMENTS

3.1. Data preparation

In this study, our dataset is derived from T1w images sourced from the Human Connectome Project (HCP) dataset, comprising 1,113 participants. We conducted experiments on a randomly selected subset of 300 participants. This subset was divided into distinct groups, including the source group (120 participants), the target group (120 participants), the validation group (30 participants), and the evaluation group (30 participants). The four groups were isolated from the others. To assess the model’s performance under varying amounts of HR samples and dependence on HR data, we further curated new source groups by selecting 70%, 50%, 30%, and 10% of participants from the source group. The target group underwent down-sampling using 3D K-space truncation with a scale factor of $2 \times 2 \times 2$.

3.2. Experimental Setup

We employed several state-of-the-art UL methods for comparison, including ZSSR [24], DASR [10], Pseudo SR [9], Blind SR [11], and UDEAN [12]. All these methods utilized the TS-RCAN network [6] as their underlying architecture and adopted hyperparameter settings in line with those of UDEAN to ensure equitable comparisons. To expedite the training process of our model, we utilized the distributed data-parallel method, training the model on two NVIDIA GeForce RTX 3090 GPUs. Our deep learning framework included PyTorch 1.9 and Lightning 2.0. For stable training, we set the learning rate of the discriminator to 0.00005 and that of the generator to 0.0002. We employed two well-established metrics: the peak signal-to-noise ratio (PSNR) and the structure similarity index (SSIM) to evaluate the image quality.

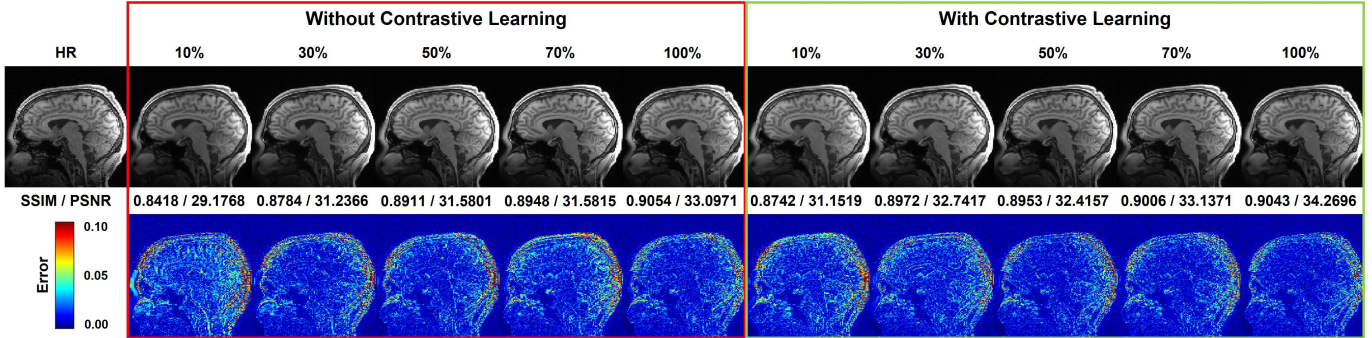


Fig. 2. Qualitative comparison in visual effect and error maps with various HR MRI images. The visualization results in the sagittal plane of the HCP dataset with a scale factor of $2 \times 2 \times 2$.

Table 1. Quantitative comparison with other reconstruction methods on the HCP dataset.

Model name	Learning	SSIM	PSNR
Tricubic	-	0.8981 ± 0.0106	31.5862 ± 1.8520
ZSSR[24]	UL	0.8994 ± 0.0163	33.0213 ± 2.2054
DASR[10]	UL	0.8931 ± 0.0094	32.3309 ± 1.4671
Pseudo SR [9]	UL	0.8931 ± 0.0116	31.0407 ± 1.8816
Blind-SR [11]	UL	0.9132 ± 0.0100	33.0695 ± 1.4656
UDEAN [12]	UL	0.9231 ± 0.0083	33.2484 ± 1.8029
Ours	CL	0.9195 ± 0.0077	33.9776 ± 1.7226

3.3. Results and Analysis

3.3.1. Comparison with state-of-the-art UL MRI SR models

Table 1 presents the numerical experimental results, demonstrating that our proposed model outperforms the comparison algorithms in nearly all cases. Notably, our model exhibits superior consistency, with the most minor standard deviation observed in both SSIM and PSNR metrics. Furthermore, as a UL approach, our model significantly surpasses the SL model Tricubic. Specifically, while our model’s SSIM is slightly lower than that of UDEAN (by 0.0036), it achieves a substantial PSNR improvement of 0.7292 dB.

3.3.2. Comparison of different numbers of HR images

To assess our model’s performance under clinical conditions with limited HR training samples, we conducted experiments with varying numbers of HR images for training, and the corresponding test results are depicted in Fig. 3. Additionally, we explored the impact of CL by removing the contrastive loss from our model.

Fig. 3 highlights that both our proposed model with and without the contrastive loss achieve high SSIM and PSNR values when an adequate number of HR samples are available. However, as the number of accessible HR images diminishes, the inclusion of the contrastive loss enhances the model’s stability. Notably, in the scenario with only 10% (12 HR MRI images) training samples, the CL-based model out-

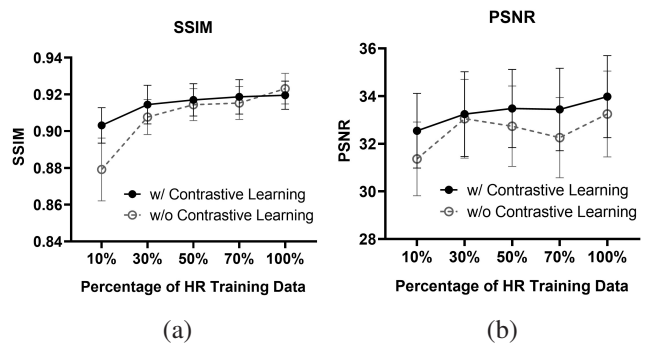


Fig. 3. Performance of models with varied numbers of HR images. (a) and (b) are SSIM and PSNR results of ablation on contrastive loss, respectively.

performs its counterpart by a notable margin, achieving improvements of 0.0239 in SSIM and 1.1802 dB in PSNR. In the qualitative comparison shown in Fig. 2, we can also observe the same phenomenon. As the number of training samples decreases, the generated SR images become increasingly blurry. As shown in the error maps, the model achieves the best accuracy and lower errors when adding contrastive loss.

4. CONCLUSION

This study introduces a novel unpaired MRI SR network that harnesses self-supervised CL and an efficient strategy for constructing positive and negative sample pairs. Our experimental findings underscore the efficacy of CL in enhancing the model’s inference stability. Notably, our model excels in scenarios with limited HR image availability, showcasing its robust performance. It is important to note that our proposed model employs a straightforward approach for constructing positive and negative sample pairs. Future research will delve into more sophisticated sample pair construction and data augmentation strategies to further enhance the model’s inference capabilities.

5. REFERENCES

- [1] Y Li, Bruno Sixou, and F Peyrin, "A review of the deep learning methods for medical images super resolution problems," *Irbm*, vol. 42, no. 2, pp. 120–133, 2021.
- [2] Jakub Jurek, Marek Kociński, Andrzej Materka, Marcin Elgalal, and Agata Majos, "Cnn-based superresolution reconstruction of 3d mr images using thick-slice scans," *Biocybernetics and Biomedical Engineering*, vol. 40, no. 1, pp. 111–125, 2020.
- [3] Jiangjie Wu, Lixuan Chen, Zhenghao Li, Lihui Wang, Rongpin Wang, Hongjiang Wei, and Yuyao Zhang, "Assured: A self-supervised deep decoder network for fetus brain mri reconstruction," in *2023 IEEE 20th International Symposium on Biomedical Imaging (ISBI)*. IEEE, 2023, pp. 1–5.
- [4] Yuhua Chen, Yibin Xie, Zhengwei Zhou, Feng Shi, Anthony G Christodoulou, and Debiao Li, "Brain mri super resolution using 3d deep densely connected neural networks," in *2018 IEEE 15th international symposium on biomedical imaging (ISBI 2018)*. IEEE, 2018, pp. 739–742.
- [5] Xiaole Zhao, Yulun Zhang, Tao Zhang, and Xueming Zou, "Channel splitting network for single mr image super-resolution," *IEEE transactions on image processing*, vol. 28, no. 11, pp. 5649–5662, 2019.
- [6] Hao Li and Jianan Liu, "3d high-quality magnetic resonance image restoration in clinics using deep learning," *arXiv preprint arXiv:2111.14259*, 2021.
- [7] Jun-Yan Zhu, Taesung Park, Phillip Isola, and Alexei A Efros, "Unpaired image-to-image translation using cycle-consistent adversarial networks," in *Proceedings of the IEEE international conference on computer vision*, 2017, pp. 2223–2232.
- [8] Yuan Yuan, Siyuan Liu, Jiawei Zhang, Yongbing Zhang, Chao Dong, and Liang Lin, "Unsupervised image super-resolution using cycle-in-cycle generative adversarial networks," in *Proceedings of the IEEE conference on computer vision and pattern recognition workshops*, 2018, pp. 701–710.
- [9] Yunxuan Wei, Shuhang Gu, Yawei Li, Radu Timofte, Longcun Jin, and Hengjie Song, "Unsupervised real-world image super resolution via domain-distance aware training," in *Proceedings of the IEEE/CVF Conference on Computer Vision and Pattern Recognition (CVPR)*, June 2021, pp. 13385–13394.
- [10] Shunta Maeda, "Unpaired image super-resolution using pseudo-supervision," in *Proceedings of the IEEE/CVF Conference on Computer Vision and Pattern Recognition (CVPR)*, June 2020.
- [11] Hexiang Zhou, Yawen Huang, Yuexiang Li, Yi Zhou, and Yefeng Zheng, "Blind super-resolution of 3d mri via unsupervised domain transformation," *IEEE Journal of Biomedical and Health Informatics*, vol. 27, no. 3, pp. 1409–1418, 2023.
- [12] Jianan Liu, Hao Li, Tao Huang, Euijoon Ahn, Adeel Razi, and Wei Xiang, "Unsupervised representation learning for 3d mri super resolution with degradation adaptation," *arXiv preprint arXiv:2205.06891*, 2022.
- [13] Kaiming He, Haoqi Fan, Yuxin Wu, Saining Xie, and Ross Girshick, "Momentum contrast for unsupervised visual representation learning," in *Proceedings of the IEEE/CVF conference on computer vision and pattern recognition*, 2020, pp. 9729–9738.
- [14] Ting Chen, Simon Kornblith, Mohammad Norouzi, and Geoffrey Hinton, "A simple framework for contrastive learning of visual representations," in *International conference on machine learning*. PMLR, 2020, pp. 1597–1607.
- [15] Jean-Bastien Grill, Florian Strub, Florent Altché, Corentin Tallec, Pierre Richemond, Elena Buchatskaya, Carl Doersch, Bernardo Avila Pires, Zhaohan Guo, Mohammad Gheshlaghi Azar, et al., "Bootstrap your own latent—a new approach to self-supervised learning," *Advances in neural information processing systems*, vol. 33, pp. 21271–21284, 2020.
- [16] Xinlei Chen and Kaiming He, "Exploring simple siamese representation learning," in *Proceedings of the IEEE/CVF conference on computer vision and pattern recognition*, 2021, pp. 15750–15758.
- [17] Gang Wu, Junjun Jiang, and Xianming Liu, "A practical contrastive learning framework for single-image super-resolution," *IEEE Transactions on Neural Networks and Learning Systems*, 2023.
- [18] Ziwei Luo, Haibin Huang, Lei Yu, Youwei Li, Haoqiang Fan, and Shuaicheng Liu, "Deep constrained least squares for blind image super-resolution," in *Proceedings of the IEEE/CVF Conference on Computer Vision and Pattern Recognition*, 2022, pp. 17642–17652.
- [19] Yanbo Wang, Shaohui Lin, Yanyun Qu, Haiyan Wu, Zhizhong Zhang, Yuan Xie, and Angela Yao, "Towards compact single image super-resolution via contrastive self-distillation," *arXiv preprint arXiv:2105.11683*, 2021.
- [20] Jiahui Zhang, Shijian Lu, Fangneng Zhan, and Yingchen Yu, "Blind image super-resolution via contrastive representation learning," *arXiv preprint arXiv:2107.00708*, 2021.
- [21] Yanqiao Zhu, Yichen Xu, Feng Yu, Qiang Liu, Shu Wu, and Liang Wang, "Deep graph contrastive representation learning," *arXiv preprint arXiv:2006.04131*, 2020.
- [22] Yulun Zhang, Kunpeng Li, Kai Li, Lichen Wang, Bineng Zhong, and Yun Fu, "Image super-resolution using very deep residual channel attention networks," in *Proceedings of the European conference on computer vision (ECCV)*, 2018, pp. 286–301.
- [23] Longguang Wang, Yingqian Wang, Xiaoyu Dong, Qingyu Xu, Jungang Yang, Wei An, and Yulan Guo, "Unsupervised degradation representation learning for blind super-resolution," in *Proceedings of the IEEE/CVF Conference on Computer Vision and Pattern Recognition*, 2021, pp. 10581–10590.
- [24] Assaf Shocher, Nadav Cohen, and Michal Irani, "zero-shot" super-resolution using deep internal learning," in *Proceedings of the IEEE Conference on Computer Vision and Pattern Recognition (CVPR)*, June 2018.